J|A|C|S
ARTICLES
Published on Web 12/15/2006

Charge Recombination versus Charge Separation in Donor−Bridge−Acceptor Systems

Joanna Wiberg,[†] Lijun Guo,[†,§] Karin Pettersson,[†] Daniel Nilsson,[‡] Thomas Ljungdahl,[‡] Jerker Mårtensson,[‡] and Bo Albinsson*[,†]

Contribution from the Department of Chemical and Biological Engineering/Physical Chemistry and Department of Organic Chemistry, Chalmers University of Technology, SE-412 96 Göteborg, Sweden

Received September 1, 2006; E-mail: balb@chalmers.se

Abstract: Optimizing the ratio of the rates for charge separation (CS) over charge recombination (CR) is crucial to create long-lived charge-separated states. Mastering the factors that govern the electron transfer (ET) rates is essential when trying to achieve molecular-scale electronics, artificial photosynthesis, and also for the further development of solar cells. Much work has been put into the question of how the donor−acceptor distances and donor−bridge energy gaps affect the electronic coupling, V_{DA}, and thus the rates of ET. We present here a unique comparison on how these factors differently influence the rates for CS and CR in a porphyrin-based donor−bridge−acceptor model system. Our system contains three series, each of which focuses on a separate charge-transfer rate-determining factor, the donor−acceptor distance, the donor−bridge energy gap, and last, the influence of the electron acceptor on the rate for charge transfer. In these three series both CS and CR are governed by superexchange interactions which make a CR/CS comparative study ideal. We show here that the exponential distance dependence increases slightly for CR compared to that for CS as a result of the increased tunneling barrier height for this reaction, in accordance with the McConnell superexchange model. We also show that the dependence on the tunneling barrier height is different for CS and CR. This difference is highly dependent on the electron acceptor and thus cannot solely be explained by the differences in the frontier orbitals of the electron donor in these porphyrin systems.

Introduction

The effect of donor−acceptor distance, R_{DA}, and donor−bridge energy gap, ΔE, on the rate of photoinduced electron transfer, ET, has been studied intensely.[1−9] Our research group has previously reported on how these two variables interplay in their influence on the rate for charge separation in a set of ZnP−*n*B/RB−AuP$^+$ donor−bridge−acceptor, D−B−A, molecules.[4,10] Now, the same set is studied with focus on the subsequent charge recombination. Since both charge separation, CS, and charge recombination, CR, in these systems are governed by the superexchange mechanism, this series of molecules provides a unique possibility to study how and why the ET dependency on barrier width and height might change when going from CS to CR. Thus, a full comparison can be made on how these processes are differently influenced by R_{DA}, ΔE, and the electron acceptor.

The rate of the CS studied in our previous work showed an exponential distance dependence with an attenuation factor $\beta = 0.31$ Å^{-1} in DMF.[10] Further, the electronic coupling between donor and acceptor, V_{DA}, showed a linear dependence on $1/\Delta E$.[4] By comparing these dependencies for CS with those found for CR, much information can be gained on how to optimize D−B−A systems to achieve long-lived charge-separated species with high quantum yield for photoinduced ET.

The presently studied D−B−A systems are divided into three series, series **1**−**3** as presented in Chart 1. We use zinc(II) 5,-15-diaryl-2,8,12,18-tetraethyl-3,7,13,17-tetramethylporphyrin (ZnP) as electron donor and the corresponding gold(III) tetrafluoroborate porphyrin (AuP$^+$) as electron acceptor in series **1** and series **2**. Series **1** contains the bridges 2B, 3B, 4B, and 5B where 2−5 refers to the number of phenyl groups in the bridge giving a R_{DA} that varies from 19.7 to 40.3 Å^{-1} (center-to-center distance).[11] In contrast, the R_{DA} remains constant (26.5 Å)

[†] Department of Chemical and Biological Engineering/Physical Chemistry.
[‡] Department of Organic Chemistry.
[§] Present address: Physics Department of Henan University, Kaifeng 475001, P.R. China.

(1) Weiss, E. A.; Ahrens, M. J.; Sinks, L. E.; Gusev, A. V.; Ratner, M. A.; Wasielewski, M. R. *J. Am. Chem. Soc.* **2004**, *126*, 5577−5584.
(2) Portela, C. F.; Brunckova, J.; Richards, J. L.; Schöllhorn, B.; Iamamoto, Y.; Magde, D.; Traylor, T. G.; Perrin, C. L. *J. Phys. Chem. A* **1999**, *103*, 10540−10552.
(3) Closs, G. L.; Miller, J. R. *Science* **1988**, *240*, 440−447.
(4) Kilså, K.; Kajanus, J.; Macpherson, A. N.; Mårtensson, J.; Albinsson, B. *J. Am. Chem. Soc.* **2001**, *123*, 3069−3080.
(5) Helms, A.; Heiler, D.; McLendon, G. *J. Am. Chem. Soc.* **1992**, *114*, 6227−6238.
(6) Osuka, A.; Tanabe, N.; Kawabata, S.; Yamazaki, I.; Nishimura, Y. *J. Org. Chem.* **1995**, *60*, 7177−7185.
(7) Paddon-Row, M. N.; Oliver, A. M.; Warman, J. M.; Smit, K. J.; De, Haas, M. P.; Oevering, H.; Verhoeven, J. W. *J. Phys. Chem.* **1988**, *92*, 6958−6962.
(8) Davis, W. B.; Svec, W. A.; Ratner, M. A.; Wasielewski, M. R. *Nature* **1998**, *396*, 60−63.
(9) Heitele, H.; Michel-Beyerle, M. E.; Finckh, P. *Chem. Phys. Lett.* **1987**, *134*, 273−278.
(10) Pettersson, K.; Wiberg, J.; Ljungdahl, T.; Mårtensson, J.; Albinsson, B. *J. Phys. Chem. A* **2006**, *110*, 319−326.

Chart 1 Studied D−B−A Systems Divided into Three Series; Series **1**: ZnP−*n*B−AuP$^+$, Series **2**: ZnP−RB−AuP$^+$, and Series **3**: Zn(Im)P−RB−Fe(Im)$_2$P and the Reference Substances ZnP−*n*B and AuP$^+$

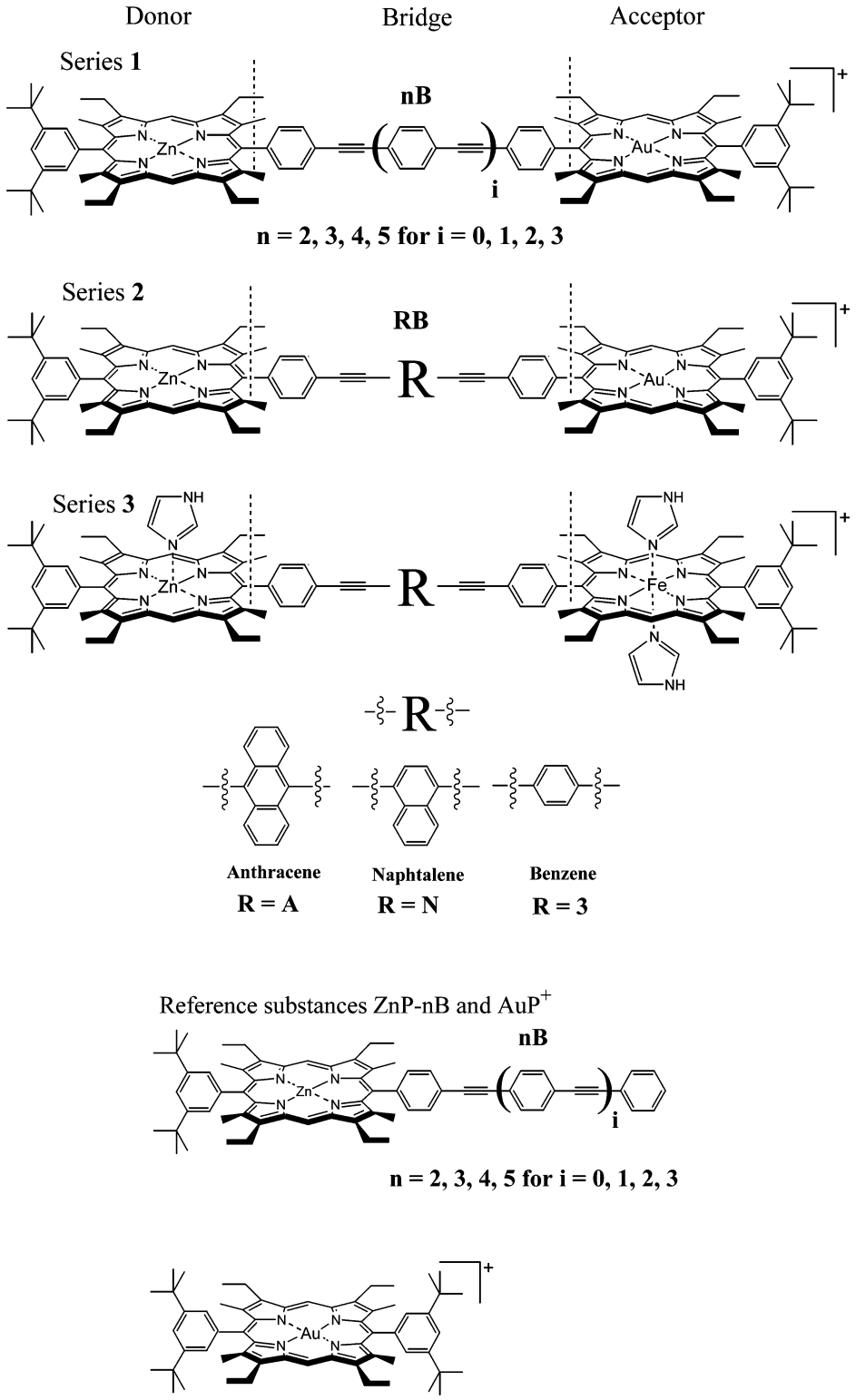

throughout series **2**. This series is designed to explore the D−B energy gap dependence and the energy gap, ΔE, within this series ranges from 3900 cm^{-1} (AB) to 11600 cm^{-1} (3B) for CS.[4] ZnP−3B−AuP$^+$ is consequently a member of both series **1** and series **2**.

Series **3**, is a parallel series of series **2** in which the electron acceptor is changed to an iron(III) porphyrin with two imidazole ligands coordinated to the iron (Fe(Im)$_2$P). By adding imidazole to the solution of the corresponding high-spin complex (Fe(Cl)P) a low-spin state of iron(III) is produced, which was shown to be essential for ET to be a competitive process in this system.[12] These sets of D−B−A molecules will thus provide

(11) Eng, M. P.; Ljungdahl, T.; Mårtensson, J.; Albinsson, B. *J. Phys. Chem. B* **2006**, *110*, 6483−6491.

the possibility of a full study in three dimensions of the potential differences in the influence of barrier width and height as well as electron acceptor on V_{DA} for CS and CR, respectively.

Materials and Methods

Materials. The synthesis of all the compounds used in this study has been reported previously.[4,13−16] All solvents were of analytical grade, and the solvents used for the lifetime measurements—dimethylformamide (DMF) and 2-methyltetrahydrofuran (2-MeTHF)—were used as purchased. The solvent used for the electrochemical measurements, tetrahydrofuran (THF), was distilled to remove stabilizers and water and thereafter stored with molecular sieve. Acetonitrile was distilled and used as solvent in the reference electrode. Tetrabutylammonium perchlorate (TBAP) and $AgNO_3$ were used as purchased.

Absorption Spectra were recorded on either a Cary 4 or a Cary 4 Bio prior to and after all lifetime measurements to establish the purity and concentration of the samples.

Nanosecond Transient Absorption was measured after excitation with a <7-ns (full width at half-maximum) laser pulse from a pulsed Nd:YAG laser (Continuum Surelite II-10) which was sent through an OPO (Surelite) to tune the wavelength to 548 nm. The light from a pulsed xenon lamp was sent through the sample perpendicular to the laser radiation and used as a probe. The probe light was then sent through a monochromator and registered by a five-stage Hamamatsu R928 photomultiplier tube. Sixteen transient signals and baseline signals were collected at 680 nm (to detect the kinetics of the $ZnP^{\bullet+}$ radical) and were averaged by a 200 MHz digital oscilloscope (Tektronix TDS2200 2 Gs/s). A LabView program was used to store the signals and to control the whole system. All samples were degassed by about five freeze−pump−thaw cycles to a pressure $<10^{-4}$ mbar before the measurements. The ground-state absorbance at the excitation wavelength at the ZnP Q-band peak was kept below 0.2.

Femtosecond Transient Absorption was measured after exciting the ZnP Q-band peak maximum at 545−548 nm, depending on solvent and molecule studied with a <200-fs laser pulse from the output of a TOPAS (Light Conversion Ltd.) pumped by a Ti:sapphire regenerative amplifier (Spitfire, Spectra Physics). The amplifier was pumped by a Q-switched diode-pumped Nd:YLF laser (EvolutionX, Spectra Physics) and seeded by a mode-locked Ti:sapphire laser (Tsunami, Spectra Physics) pumped by a frequency-doubled diode-pumped Nd:YVO_4 laser (Millennia VS, Spectra Physics). The output from the regenerative amplifier was split into two beams by a 70/30 beamsplitter: 70% going through the TOPAS and 30% was after passing two OD filters (one with OD 4 and one variable 0−2) sent through a sapphire plate to produce the white light continuum used as probe light. The output from the TOPAS, which was used as a pump beam, was chopped at 500 Hz to block every other pulse and was sent through a homemade computer-controlled optical delay line before being focused on the sample with reflective optics. As rather large delay times were used, the small loss of collimation of the pump beam introduced by the TOPAS was compensated for by the use of a telescope. To compensate for any instability in the produced white light, a 50/50 beamsplitter was used to divide the white light into a probe and a reference beam. The probe beam was overlapping the pump beam at the sample, while the reference beam was sent through the sample at a small separation from the pump and the probe beams. The probe and reference beams were sent trough a monochromator (ISA, TRIAX 180), and the signals were registered by two Si-photodiodes. A third photodiode was used to monitor the pump beam. All signals were gated by boxcar integrators (SR250, Stanford Research Systems), fed into a PC-based AD card, and averaged by a LabView program. The samples were kept in 1- or 2-mm cuvettes, and the ground-state absorption at the excitation wavelength was kept between 0.7 and 0.9, while the pulse energy was around 3 μJ/pulse.

Electrochemical Measurements were performed on the *n*B bridge molecules and ZnP by means of cyclic voltammetry, CV, and differential pulse voltammetry, DPV, using ferrocene as an internal standard. All measurements were carried out with a platinum working electrode, a platinum counter electrode, and an Ag/Ag^+ reference electrode. The inner solution of the reference electrode was a mix of 0.1 M TBAP and 10 mM $AgNO_3$ in acetonitrile. The measurements were made in dried THF which was degassed with N_2 prior to all measurements, and 0.1 M TBAP was used as supporting electrolyte. The sample concentration was 2 mM. The steps for DPV were between 1 and 4 mV, and the sweeping rate for CV was between 10 and 100 mV/s.

Results

The purpose of this study is to compare the influence of bridge length and bridge energy on the CR rate with that for the CS rate in different D−B−A systems, as well as to investigate the influence of the electron acceptor on these rates. The lifetimes of the charge-separated states were obtained through transient absorption measurements on three sets (Chart 1) of D−B−A molecules: series **1**: the ZnP−*n*B−AuP^+ series, with R_{DA} ranging from 19.7 to 40.3 Å (center-to-center) estimated from DFT calculations.[11] Series **2**: the ZnP−RB−AuP^+ series, with constant R_{DA} = 26.5 Å but with different donor−bridge energy gaps, and series **3**: the Zn(Im)P−RB−$Fe(Im)_2P$ series which is similar to series **2** but with the metalation state of the acceptor changed. Through the recombination rates and estimations of the driving forces, ΔG^0, and the reorganization energies, λ, the electronic coupling between the charge-separated state and the ground state is calculated from the Marcus equation (eq 5).[17] The difference in the electronic coupling between the CS and the CR process will be analyzed in the Discussion following this section.

It is also of interest whether the studied recombination process has the character of hole transfer, HT, or ET. Electrochemical measurements were hence performed on the *n*B bridges in order to get a full energy level diagram of the states involved.

Ground-State Absorption spectra, Figure 1, show the characteristic porphyrin Sôret-band centered around 400 nm and the much less intense Q-band around 550 nm with the main peak being the ZnP Q(1,0) transition (at 548 nm in DMF). The spectra of the D−B−A dimers are essentially the sum of the spectra of the D−B references and A, which indicates that the electronic properties of the D, B, and A moieties in the dimers are preserved.

Transient Absorption measurements were performed on all the investigated molecules to probe the recombination process $D^{\bullet+}-B-A^{\bullet-} \rightarrow D-B-A$ after excitation in the Q(1,0) band. The recombination rates were measured by following the decay of $ZnP^{\bullet+}$, which has a characteristic absorption at 680 nm.[10,18−21] In a typical measurement, the ΔA signal at 680 nm was between

(12) Pettersson, K.; Kilså, K.; Mårtensson, J.; Albinsson, B. *J. Am. Chem. Soc.* **2004**, *126*, 6710−6719.
(13) Ljungdahl, T.; Pettersson, K.; Albinsson, B.; Mårtensson, J. *J. Org. Chem.* **2006**, *71*, 1677−1687.
(14) Kilså, K.; Kajanus, J.; Larsson, S.; Macpherson, A. N.; Mårtensson, J.; Albinsson, B. *Chem. Eur. J.* **2001**, *7*, 2122−2133.
(15) Kajanus, J.; Van Berlekom, S. B.; Albinsson, B.; Mårtensson, J. *Synthesis* **1999**, 1155−1162.
(16) Kilså, K.; Kajanus, J.; Mårtensson, J.; Albinsson, B. *J. Phys. Chem. B* **1999**, *103*, 7329−7339.
(17) Marcus, R. A. *J. Chem. Phys.* **1956**, *24*, 966−978.
(18) Fajer, J.; Borg, D. C.; Forman, A.; Dolphin, D.; Felton, R. H. *J. Am. Chem. Soc.* **1970**, *92*, 3451−3459.
(19) Andréasson, J.; Kodis, G.; Ljungdahl, T.; Moore, A. L.; Moore, T. A.; Gust, D.; Mårtensson, J.; Albinsson, B. *J. Phys. Chem. A* **2003**, *107*, 8825−8833.

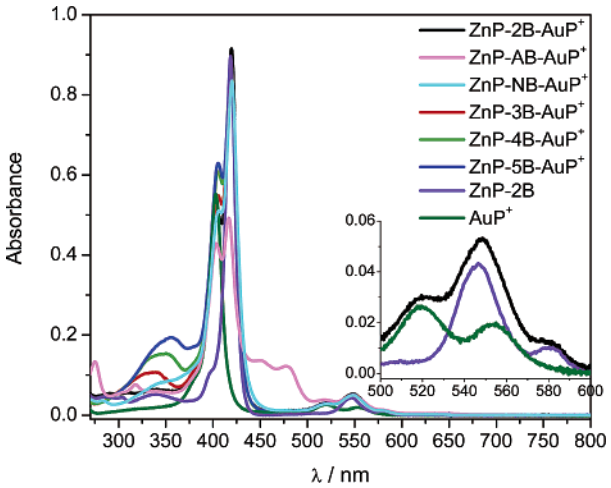

Figure 1. Absorption spectra of series **1**, series **2**, and the reference compounds ZnP−2B and AuP^+ in DMF. (Inset) In the Q-band region the absorption spectrum of ZnP−*n*B−AuP^+ is essentially the sum of the spectra of ZnP−*n*B and AuP^+.

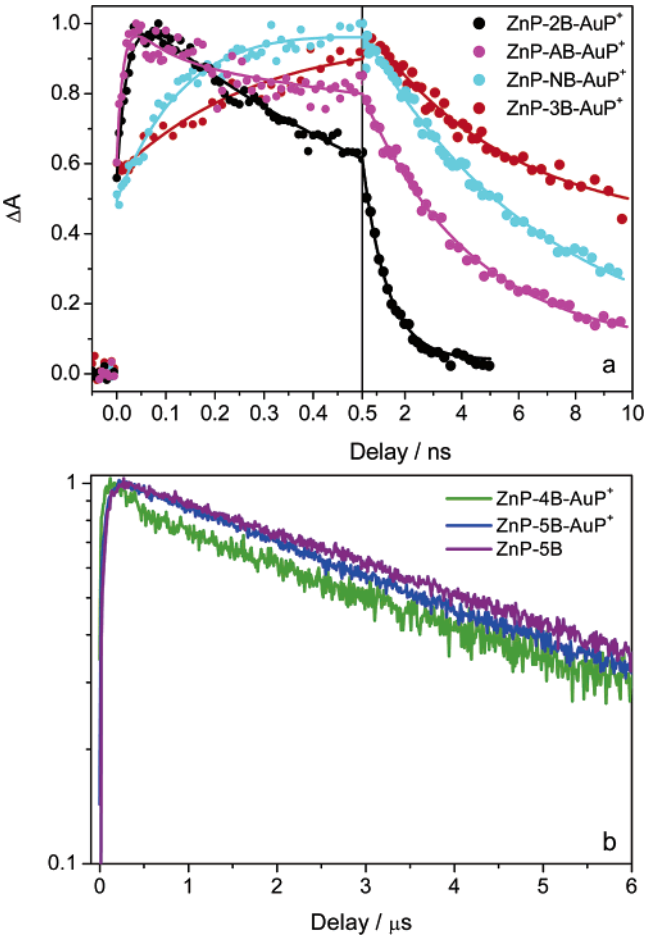

Figure 2. Transient absorption traces at 680 nm of series **1** and series **2** in DMF after excitation in the ZnP *Q*(1,0) band with (a) <200-fs laser pulses, and (b) <7-ns laser pulses. Note that, for clarity, the Δ*A* scale is logarithmic in panel b.

0.008 and 0.030, depending on the quantum yield for the charge separation. However, the transient decay traces, presented in Figure 2, are normalized for clarity. Transient absorption measurements were also performed on the reference substances ZnP−*n*B, probing at 680 nm where the excited states ^{1}ZnP and ^{3}ZnP have weak absorption.[22] The kinetics of ZnP−*n*B at 680 nm showed the expected 1.46 ns excited-state lifetime of ^{1}ZnP,[10] and at longer times a biexponential decay in agreement with the conformational dynamics reported for the two states of ^{3}ZnP—a buildup time of about 60 ns followed by a 5.6 μs decay,[23] all in DMF.

Table 1. Rates for Charge Separation and Charge Recombination in Series **1**−**3**

series	R_{DA}/Å	molecule	solvent	$(k_{CS})^{-1}$/ps	$(k_{CR})^{-1}$/ns
1	19.7	ZnP−2B−AuP^+	DMF	37[a]	0.88 ± 0.02[b]
2	26.5	ZnP−AB−AuP^+	DMF	33[c]	3.7 ± 0.2[b]
2	26.5	ZnP−NB−AuP^+	DMF	223[d]	6 ± 1[b]
1, 2	26.5	ZnP−3B−AuP^+	DMF	394[a]	6 ± 1[b]
1	33.4	ZnP−4B−AuP^+	DMF	3642[a]	210 ± 30[e]
1	40.3	ZnP−5B−AuP^+	DMF	22352[a]	2100 ± 200[e]
3	26.5	Zn(Im)P−AB−$Fe(Im)_2$P	2-MeTHF	62.5[f]	0.48[b]
3	26.5	Zn(Im)P−NB−$Fe(Im)_2$P	2-MeTHF	526[f]	1.25[b]
3	26.5	Zn(Im)P−3B−$Fe(Im)_2$P	2-MeTHF	1111[f]	1.72[b]

[a] From ref 10. [b] Measured with fs transient absorption. [c] From ref 27. [d] From ref 4. [e] Measured with ns transient absorption. [f] From ref 12.

For ZnP−2B−AuP^+ and ZnP−3B−AuP^+ the measured kinetics were fitted to a biexponential expression, where the two lifetimes correspond to the singlet excited-state lifetime of ZnP, dominated by the rate for CS, and the rate for CR respectively. The CS quantum yields are lower for ZnP−4B−AuP^+ and ZnP−5B−AuP^+ and therefore only a small part of the signal at 680 nm will be from the radical species,[10] while the signals from ^{3}ZnP should be clearly visible. From Figure 2b it is evident that this is just the case, and at long times (t > 10 ns) a three-exponential expression was thus fitted to the kinetics at 680 nm for these dimers (two for ^{3}ZnP and one for the $ZnP^{\bullet+}$ species). The charge-separated state lifetimes are presented in Table 1. In addition, the two lifetimes associated with ^{3}ZnP show for both the longest dimers a perfect match with those for ZnP−*n*B at longer delay times. Thus, no quenching of the ^{3}ZnP state is observed although the CS process is thermodynamically feasible also from this state (cf. Figure 3).

As the CR process competes with no other deactivation process, the rate constants for CR will just be the inverse of the measured charge-separated state lifetimes (eq 1, Table 1) ,

$$k_{CR} = \frac{1}{\tau_{CS}} \qquad (1)$$

It is apparent from Figure 2 that the recombination process has strong distance dependence since the charge-separated state lifetimes differ by 3 orders of magnitude in series **1**. Clearly, the D−B−A molecule with the shortest bridge, 2B, shows the fastest recombination rate, whereas the molecule with the longest bridge, 5B, shows the slowest recombination rate. For series **2** and series **3** the difference between the recombination rates is significant but much smaller than in series **1**. The CR rate decreases in both series going from the system with the AB-

(20) Imahori, H.; Hagiwara, K.; Aoki, M.; Akiyama, T.; Taniguchi, S.; Okada, T.; Shirakawa, M.; Sakata, Y. *J. Am. Chem. Soc.* **1996**, *118*, 11771−11782.
(21) Chosrowjan, H.; Tanigichi, S.; Okada, T.; Takagi, S.; Arai, T.; Tokumaru, K. *Chem. Phys. Lett.* **1995**, *242*, 644−649.
(22) Rodriguez, J.; Kirmaier, C.; Holten, D. *J. Am. Chem. Soc.* **1989**, *111*, 6500−6506.
(23) Andréasson, J.; Zetterqvist, H.; Kajanus, J.; Mårtensson, J.; Albinsson, B. *J. Phys. Chem. A* **2000**, *104*, 9307−9314.

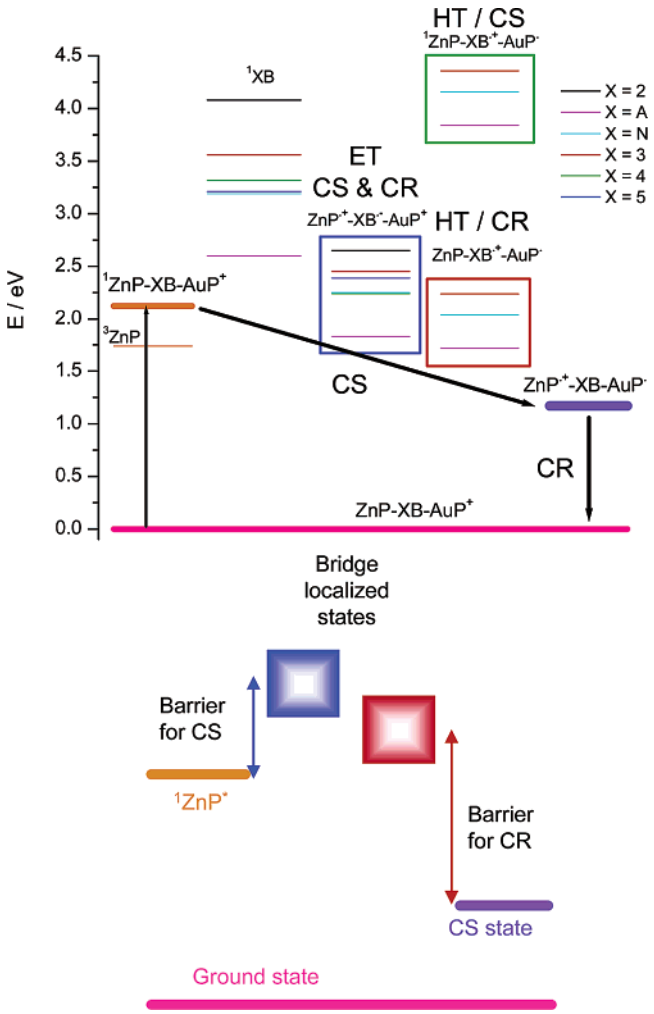

Figure 3. (Top) Energy level diagram of the states of interest for series **1** and series **2** in DMF. The ET pathway for both CS and CR uses the virtual state ZnP$^{\bullet+}$−XB$^{\bullet-}$−AuP$^+$ for mediation. For the corresponding HT pathways, the ZnP−XB$^{\bullet+}$−AuP$^\bullet$ and ^{1}ZnP−XB$^{\bullet+}$−AuP$^\bullet$ species are the barrier-determining states for CR and CS, respectively. For CS the HT-mediating states involve the excited-state of ZnP and are therefore well above those for ET. The energy levels of series **3** show similar features but were omitted for clarity. (Bottom) Schematic picture of the top panel, showing the increase in barrier height for the CR step. See Table S1 (Supporting Information) for numerical values of the redox potentials.

bridge, i.e., the bridge with the lowest-energy barrier, to the system with the 3B-bridge, i.e., the bridge with the highest-energy barrier.

Electrochemical Measurements were made in order to estimate whether the charge recombination has HT or ET character. Cyclic voltammetry, CV, and differential pulse voltammetry, DPV, were performed on the set of *n*B bridges to measure their reduction potentials (Table S1, Supporting Information). CV measurements showed irreversible reduction patterns for all *n*B bridges and the expected two-step reversible oxidation pattern for ZnP,[24] giving the difference between the ZnP oxidation and the bridge reduction potential [E_{ox}(ZnP) − E_{red}(B)] to be between 2.98 and 2.49 V for the bridges 2B−5B. Previous measurements gave the following values for [E_{ox}(ZnP) − E_{red}(B)] in series **2** and **3**: 2.73 V for 3B, 2.48 V for *n*B, and 2.06 V for AB.[4]

(24) Kilså, K.; Macpherson, A. N.; Gillbro, T.; Mårtensson, J.; Albinsson, B. *Spectrochim. Acta A* **2001**, *57*, 2213−2227.

Using the redox potentials of the XB bridges (XB is the common term for both the *n*B and RB bridges) and the porphyrin moieties, a full energy level diagram of states with either a reduced or oxidized bridge is presented in Figure 3 (top). Although the electron will never reside on the bridge, the order of these states should give an idea of what kind of process has the major part in mediating the charge recombination. For HT the energy barrier through which the electron tunnels is associated with the ZnP−XB$^{\bullet+}$−AuP$^\bullet$ state, i.e., with the oxidation potential of the XB-bridge. In the same way the barrier height for ET is related to the ZnP$^{\bullet+}$−XB$^{\bullet-}$−AuP$^+$ state. The energies of these states have been calculated with the Weller expression, eq 2,[25]

$$E = e(E_{ox}(\mathrm{XB}) - E_{red}(\mathrm{AuP}^+)) + \frac{e^2}{4\pi\epsilon_0}\left(\frac{1}{2R^+} + \frac{1}{2R^-}\right)\left(\frac{1}{\epsilon_s} - \frac{1}{\epsilon_r}\right) \quad (2)$$

where e is the unit charge, $R^\pm$ are the radii of the radical ions,[26] ϵ_s is the dielectric constant for the solvent used for the spectroscopic measurements, and ϵ_r is the dielectric constant for the solvent used for the electrochemical measurements. For the case of ZnP$^{\bullet+}$−XB$^{\bullet-}$−AuP$^+$, a Coulombic term as presented in eq 3 has been added, giving the total energy E' (eq 4). R_{cc} is the estimated separation of the different ion pairs.

$$E^{coul} = \frac{e^2}{4\pi\epsilon_0}\left(\frac{1}{R_{cc}^{\mathrm{D}^{\bullet+}-\mathrm{B}^{\bullet-}}} + \frac{1}{R_{cc}^{\mathrm{B}^{\bullet-}-\mathrm{A}^+}} - \frac{1}{R_{cc}^{\mathrm{D}^{\bullet+}-\mathrm{A}^+}}\right)\left(\frac{1}{\epsilon_s}\right) \quad (3)$$

$$E' = E - E^{coul} \quad (4)$$

The CS step is clearly an ET process as the barrier for HT involves the ZnP in its first excited singlet state and this barrier is therefore well above that for ET. For CR, the states for ET and HT are rather close lying and only give a small indication that HT could be more favorable. In fact it is quite likely that both processes act in parallel in the CR case. Even though, in DMF, there is a driving force for stepwise ET (hopping) in the CS step for ZnP−AB−AuP$^+$, as shown in Figure 3, in a less polar solvent such as 2-MeTHF the CS has been shown to exclusively occur through a superexchange interaction.[27] The electronic coupling for CS in this molecule has been established by a temperature study reported in ref 27, and the V_{DA} values are assumed to be solvent independent. Figure 3 (bottom) also qualitatively shows the increase in the effective barrier when comparing CR to CS.

The Electronic Coupling between donor and acceptor, V_{DA}, was calculated from the experimentally determined charge-transfer rate constants, k_{CR} and k_{CS}, using the Marcus equation for non-adiabatic electron transfer, eq 5.[17]

$$k_{ET} = \sqrt{\frac{\pi}{\hbar^2\lambda k_B T}}\,|V|^2 \exp\left(\frac{-(\Delta G^0 + \lambda)^2}{4\lambda k_B T}\right) \quad (5)$$

The driving forces, ΔG^0, and reorganization energies, λ, were estimated as described in the following section. The rate

(25) Weller, A. *Z. Phys. Chem.* **1982**, *133*, 93−98.
(26) R is 4.8 Å for the porphyrins, and for the bridges, R are approximated as half the edge-to-edge distance between the porphyrins.
(27) Winters, M. U.; Pettersson, K.; Mårtensson, J.; Albinsson, B. *Chem. Eur. J.* **2005**, *11*, 562−573.

Table 2. The Driving Force for Charge Recombination, ΔG_{CR}, the Driving Force for Charge Separation, ΔG_{CS}, the Reorganization Energy, λ, and the Electronic Coupling, V_{DA}, Calculated from Eq 5, Presented along with V_{DA} Reported for the Initial CS; λ is the Same for Both CS and CR; Solvents Were DMF for Series **1** and **2** and 2-MeTHF for Series **3**

			CR			CS	
series	R_{DA}/Å	molecule	V_{DA}/cm^{-1}	ΔG_{CR}/eV	λ/eV	ΔG_{CS}/eV	V_{DA}/cm^{-1}
1	19.7	ZnP−2B−AuP$^+$	2.23	−1.17	1.25	−0.95	15.4[a]
2	26.5	ZnP−AB−AuP$^+$	1.21	−1.17	1.34	−0.95	16[b]
2	26.5	ZnP−NB−AuP$^+$	0.95	−1.17	1.34	−0.95	8.4[c]
1, 2	26.5	ZnP−3B−AuP$^+$	0.95	−1.17	1.34	−0.95	4.8[b]
1	33.4	ZnP−4B−AuP$^+$	0.17	−1.17	1.39	−0.95	2.2[a]
1	40.3	ZnP−5B−AuP$^+$	0.06	−1.17	1.42	−0.95	1.0[a]
3	26.5	Zn(Im)P−AB−Fe(Im)$_2$P	3.3	−0.92	1.09	−1.18	8.3[d]
3	26.5	Zn(Im)P−NB−Fe(Im)$_2$P	2.1	−0.92	1.09	−1.18	2.9[d]
3	26.5	Zn(Im)P−3B−Fe(Im)$_2$P	1.8	−0.92	1.09	−1.18	2.0[d]

[a] From ref 10. [b] From ref 27. [c] From ref 4. [d] Calculated from the lifetimes given in ref 12.

constants for CS were deduced from fluorescence lifetime measurements with a reduction made for an estimated Förster energy transfer contribution as described in ref 10. These measurements were carried out in four different solvents, and an averaged V_{DA} for CS for each molecule in series **1** was given in this paper.[10] Equation 5 provides the classical description of the electron-transfer rates. Quantum mechanical treatment by Jortner and co-workers[28,29] leads to an improved expression that more accurately describes the rates at low temperatures and in the so-called Marcus inverted region (where $-\Delta G° > \lambda$). In the present case, however, the magnitude of the driving forces and reorganization energies (Table 2, vide infra) are such that both the CS and CR reactions occur under normal or barrier-free conditions, which is why the benefit of using the more advanced expression is limited.

As the recombination process in series **1** and **2**, D$^{•+}$−B−A$^•$ → D−B−A$^+$ has the character of a charge shift, the driving force for charge recombination (back transfer), ΔG_{CR}, does not depend on the D/A distance. It was therefore calculated from the oxidation and reduction potentials, E_{red}(ZnP$^+$) and E_{ox}(AuP$^•$), of donor and acceptor respectively according to eq 6 without any correction for Coulombic stabilization (cf. eq 2).

$$\Delta G_{CR} = e(E_{ox} - E_{red}) + \frac{e^2}{4\pi\epsilon_0}\left(\frac{1}{\epsilon_s} - \frac{1}{\epsilon_r}\right)\left(\frac{1}{r}\right) \qquad (6)$$

Here ϵ is the dielectric constants for the solvents used in the redox potential measurements ($\epsilon_r = 8.93$ for CH_2Cl_2) and the lifetime measurements ($\epsilon_s = 38.25$ for DMF and 6.97 for 2-MeTHF), and r is the 4.8 Å radius of the porphyrin ring. The redox potentials are collected in Table S1. For series **3** the addition of imidazole was estimated to decrease the absolute values of E_{ox} and E_{red} of ZnP and Fe(Im)$_2$P, respectively, by an amount of 0.1 eV based on the observation that adding pyridine gives a lowering of the oxidation potential of ZnP by 0.09 eV.[24] In the corresponding driving force calculations for series **3**, a Coulombic stabilization term was used (eq 3).

The reorganization energy, λ, is the sum of two parts: An inner part, λ_i, and a solvent contribution, λ_s. The inner reorganization energy is set to 0.2 eV for all three series. This value has been used before for series **1**[10] and series **2**[4] as well as in other ZnP/AuP donor−acceptor pairs[30] and is not expected to differ greatly for series **3**. The inner reorganization energies are on the whole a source of uncertainties, but any trend in the recombination rate and/or the electronic coupling will hardly be affected by small changes in λ. The total reorganization energy was calculated using the center-to-center distance between donor and acceptor, R_{cc}, the refractive index, $n = 1.431$ for DMF and 1.405 for 2-MeTHF, and the dielectric constant, ϵ_s, of the solvent used and again the radius of the porphyrin, r, according to eq 7.[17]

$$\lambda = \lambda_i + \lambda_s = \lambda_i + \frac{e^2}{4\pi\epsilon_0}\left(\frac{1}{r} - \frac{1}{R_{cc}}\right)\left(\frac{1}{n^2} - \frac{1}{\epsilon_s}\right) \qquad (7)$$

The different values of λ and ΔG^0 are presented in Table 2 along with the calculated electronic couplings V_{DA}, both for CS and for CR.

Discussion

The aim of this work has been to investigate the influence of the bridge length and the bridge energy on the recombination rate in three series of D−B−A molecules. We have previously reported on the impact of these parameters on the initial CS process.[4,10] In this paper, we make a comparison between CS and CR and their dependence on the above-mentioned parameters. The differences observed for the trends in the series of the two processes are caused by a combination of a change in driving force and electronic coupling, and also on a change in the dependency of this coupling on the energy barrier. The factors causing the difference in the electronic coupling (comparing CS and CR) is analyzed on the basis of the McConnell model for superexchange.[31] The differences not accounted for by this model is here in part rationalized by a frontier orbital approach, and in part by the uncertainty associated with the choice of correct virtual state included in the McConnell model and estimating its energy.

The Distance Dependence. The rate for CS in the length series, series **1**, has previously been shown to have exponential distance dependence following eq 8 with attenuation factor $\beta = 0.31$ Å^{-1} in DMF,[10]

$$k_{ET} \propto \exp(-\beta R_{DA}). \qquad (8)$$

In Figure 4, ln(k_{CR}) shows a linear distance dependence with a negative slope, β, of 0.39 Å^{-1}, indicating that also the CR is of superexchange character and that electron hopping does not occur. The fact that β is increased for the return of the electron is predicted from the McConnell model, according to eq 9,[32]

$$\beta = \frac{2}{R_0}\ln\left(\frac{\Delta E}{\nu}\right) \qquad (9)$$

where R_0 is the distance between the bridging subunits (the phenylene ethynylene fragment in this case), ΔE is the energy gap between the porphyrin units and the bridge, while ν is the electronic coupling between the repeating bridge units. Since ν and R_0 are parameters associated only with the bridge, they are

(28) Ulstrup, J.; Jortner, J. *J. Chem. Phys.* **1975**, *63*, 4358−4368.
(29) Jortner, J.; Bixon, M. *J. Chem. Phys.* **1988**, *88*, 167−170.
(30) Harriman, A.; Heitz, V.; Sauvage, J. P. *J. Phys. Chem.* **1993**, *97*, 5940−5946.
(31) McConnell, H. M. *J. Chem. Phys.* **1961**, *35*, 508−515.
(32) Miller, J. R.; Beitz, J. V. *J. Chem. Phys.* **1981**, *74*, 6746−6756.

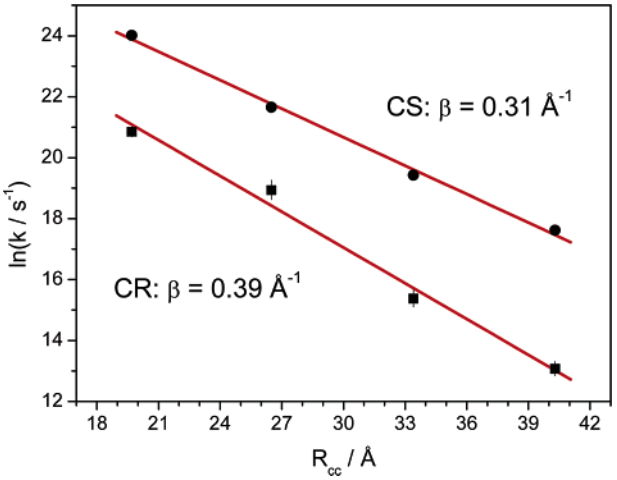

Figure 4. Exponential distance dependence of ln(k) versus R_{DA} for series **1**.

not expected to change between the CS and the CR processes, but as ΔE increases for CR (Figure 3) so should β.

The Electronic Coupling is Decreased for CR. In all three series: ZnP−*n*B−AuP$^+$, ZnP−RB−AuP$^+$, and Zn(Im)P−RB−Fe(Im)$_2$P, the electronic coupling V_{DA} for CR compared to CS is decreased, as shown in Table 2. This decrease can, according to the theory for superexchange, originate from change in the energy barrier, ΔE, and/or the electronic couplings, V_{DB} and V_{BA}, between the bridge and the D and A, respectively:

$$V_{DA} \propto \frac{V_{DB}V_{BA}}{\Delta E} \qquad (10)$$

To estimate the contributions from these two factors a plot of V_{DA} versus $1/\Delta E$ is made and shown in Figure 5. To find the proper barrier height is not straight forward, and the true value of ΔE might not be known, as it includes virtual states of the bridge, but could be approximated by calculations. Suggested ΔE's have been calculated as $\Delta E = e(E_{ox}^{D} - E_{red}^{B}) - E_{00}^{D}$,[30] or using estimations of the donor and acceptor LUMOs by employing the pairing theorem, which states that the LUMO of an organic molecule can be approximated by the sum of its excited-state energy and oxidation potential.[33] Basing the calculations on the redox potential of the bridge is highly applicable when ΔE is large, but in our systems the ionized-bridge states lie quite close to the first excited singlet state of the donor, and using redox potentials to calculate ΔE was inadequate in the case of CS for series **2**. A negative ΔE value resulted for the lowest-lying energy barrier (the AB-bridge), even in low polarity solvents although stepwise ET was not observed.[4] Consequently, a ΔE as the difference between the donor and bridge E_{00} singlet energies, which in this case is proportional to the reduction potential of the bridge, was employed for series **2**.[4]

To be able to properly compare the influence of the energy barrier between CS and CR, we have used a ΔE for CR which is calculated in the same manor as was done for CS, i.e., as the energy difference between the charge-separated state and the E_{00}'s of the bridging molecules. This probably overestimates the barrier for CR.

(33) Davis, W. B.; Ratner, M. A.; Wasielewski, M. R. *Chem. Phys.* **2002**, *281*, 333−346.

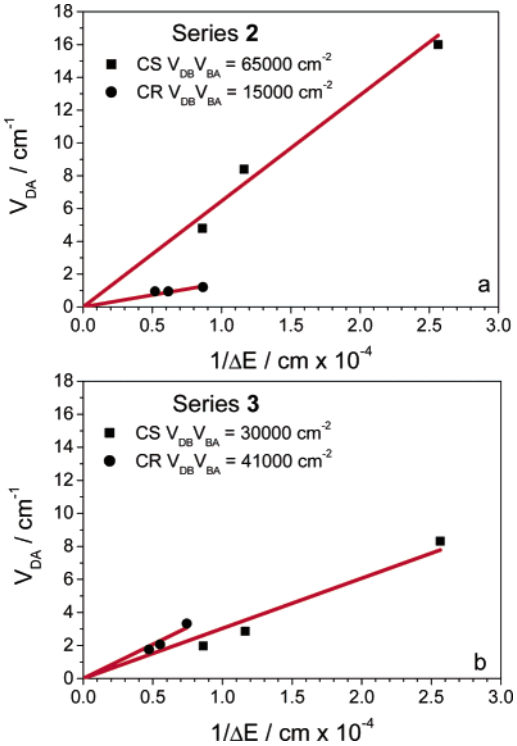

Figure 5. Electronic coupling, V_{DA}, versus the inverse energy gap between the first singlet excited-state of the donor and the bridge in (a) series **2**: ZnP−RB−AuP$^+$ and (b) series **3**: Zn(Im)P−RB−Fe(Im)$_2$P for CS (■) and CR (●). The lines are linear fits with fixed intercepts $V_{DA}(0) = 0$.

It is important to note also, the difference between the ΔE in the superexchange model and the approximations. Using redox potentials, ΔE is calculated from the energy of the *relaxed* radical species whereas the true energy barrier concerns the *unrelaxed* energy levels. The electron or hole never resides on the bridge, but tunnels through it. Using redox potentials to calculate ΔE will then give an underestimation of this barrier, whereas if ΔE is large, the difference between the virtual levels and those calculated from redox potentials or by use of the E_{00} levels is small in comparison. Conversely, if ΔE is small, the difference between the true barrier and the calculated one can become significant. Moreover, further simplifications are introduced in the superexchange model by taking into account the mediation caused by one bridge state only.[31] As for CR, the states with either an electron or a hole residing on the bridge are close-lying in energy, suggesting that assuming only one mediating state might not be as good an approximation as both HT and ET are potentially both active in the CR process.

The Electronic Coupling, Frontier Orbitals, and Reduction Sites. From the V_{DA} over $1/\Delta E$ plots in Figure 5 it is evident that the slope, $V_{DB}V_{BA}$, is much smaller for CR (15 000 cm^{-2}) than for CS (65 000 cm^{-2}) in series **2**; however, in series **3** the CR-slope (41 000 cm^{-2}) is similar to the CS-slope (30 000 cm^{-2}). The fact that the CR-slope is slightly larger than the CS-slope in series **3** could probably be attributed to larger overestimations of ΔE for CR than for CS (vide supra). However, for series **2** the large difference between the CS-slope and CR-slope must also be explained by changes in the interactions between the bridge and donor/acceptor according to eq 10. In a simplified orbital description of ET, the electron can be visualized as moving from the ZnP LUMO to the AuP$^+$ LUMO tunneling through the LUMO of the bridge. In the CR

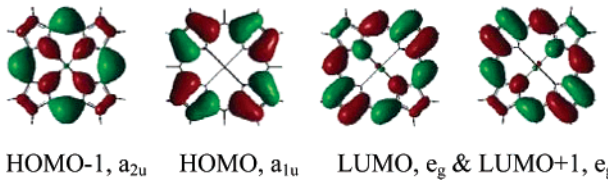

Figure 6. HOMO−1, HOMO, and the degenerated LUMO orbitals of unsubstituted ZnP.

step the electron moves from the AuP^+ LUMO to the ZnP HOMO, and in the case of HT, tunnels through the bridge HOMO.

When looking at the orbitals of the ZnP HOMO and LUMO, Figure 6, it is seen that the orbital coefficients at the *meso* carbons, where the bridge is connected, is changed from "on" in LUMO to "off" in HOMO. So, while for the CS reaction V_{DB} is related to the LUMO of the ZnP donor, the CR process should render a smaller V_{DB} as the HOMO of ZnP now is active. V_{BA} is expected to remain unchanged as the AuP^+ LUMO, which looks like the ZnP LUMO, is active in both CS and CR. It should also be added that even though there is distributional difference between the bridge HOMO and LUMO, both orbitals show considerable electron density at the porphyrin attachment points. A similar argument has been put forward to explain the large decrease in V_{DA} for CR compared to that for CS in a dimethoxynaphthalene−bridge−dicyanovinyl, D−B−A system.[34]

The lack of V_{DB} alterations in series **3** could be caused by the effect of the imidazole ligand on the porphyrin orbital distribution. It is known that the a_{1u} and a_{2u} (HOMO and HOMO−1) orbitals are very close in energy and that different substituents on the ZnP might flip the order of these two orbitals. Now, as an imidazole ligand, which also coordinates to Zn was used in series **3**, it might be that the a_{2u} orbital is the HOMO in this case. In fact, coordination to ZnP by a Lewis base is expected to raise the a_{2u} energy more than the a_{1u} energy because of the nodal pattern of these two orbitals. There should then be smaller alterations in V_{DB} when going from CS to CR when imidazole is added as the a_{2u} orbital has substantial electron density at the *meso* carbons. This hypothesis was tested on ZnP−3B−AuP^+, which is a member of both series **1** and series **2**, simply by adding imidazole to the DMF solution.[35] Adding imidazole to series **2** showed, however, no remarkable change in the factor $V_{DB}V_{BA}$ for CR. The energy levels of a_{1u} and a_{2u} of ZnP are, as said, very close lying, and since the real system lacks symmetry, a potential configurational mixing of these orbitals might occur. This could make the effect of the a_{1u}/a_{2u} ordering small.

The interpretation of the differences between series **2** and series **3** could also be based on differences in how the electron density is distributed at the electron acceptor upon reduction. Calculations on an $Fe(Im)_2P$ similar to that presently studied show a largely increased electron density on the porphyrin ring of the reduced species, indicating that the accepted electron resides on the macrocycle.[36]

The site of reduction of the AuP^+ is not equally straight forward. ESR measurements on a gold(III) 5,10,15,20-tetrakis-(3,5-di-*tert*-butylphenyl)porphyrin show a metal-centered reduction, but it could not be ruled out from those measurements that a transient radical is formed initially with the unpaired electron located on the porphyrin ring.[37] A largely decreased V_{BA} and consequently a decreased V_{DA} could be the result of the reduction of the acceptor porphyrin and the subsequent oxidation of the radical formed being located at different sites of the porphyrin. Should the CS place the transferred electron on the macrocycle of the AuP^+ followed by a very fast transfer of the electron on to the metal center (on a time scale substantially shorter than the charge-separated state lifetime), a decrease in V_{DA} for CR would be imposed.

The bottom line is that it is not sufficient to explain differences in electronic coupling for CS and CR only by looking at the initial donor frontier orbitals, but that also the differences between the electron-accepting and electron-donating orbitals of both the electron donor and acceptor are of great importance. Of concern also is the choice of correct virtual state on which the height of the energy barrier is based. The choice in our case to use the E_{00} energy of the bridge as the mediating energy level is most certainly giving overestimations of the tunneling barrier and presumably even more so for CR than for CS. Smaller ΔE for CR than the ones used will not change the situation in series **2** where there is a large decrease in the $V_{DB}V_{BA}$ factor for CR. On the contrary, should ΔE for CR be smaller, the difference would only increase. However, an increase in $1/\Delta E$ for CR could at the same time account for the small increase present in the $V_{DB}V_{BA}$ factor for CR in series **3**, shown in Figure 5.

Conclusions

The much slower charge-transfer rates in CR compared to CS cannot solely be explained by alterations in the driving force, since the values of ΔG_{CR} and ΔG_{CS} are within 0.2 eV the same for series **1** and series **2**. To further investigate the factors that influence the relative transfer rates for CR and CS, the electronic coupling was calculated from the Marcus equation. In series **1** and series **2** we showed that the electronic coupling was significantly decreased for CR within these series, while the decrease in series **3** was small. For series **2** it was clear that there were effects on the D−B−A interactions, which could not be explained by the increase in ΔE.

We have suggested an interpretation which takes into account the different electron density distributions in the ZnP HOMO and LUMO in which the node at the *meso* position of the ZnP HOMO could potentially lower the coupling between donor and bridge. The lack of such an effect in series **3** was first suggested to be a result of the possible flip in the order of the a_{1u} and a_{2u} HOMO and HOMO−1 of ZnP caused by the imidazole ligand. This assumption was not verified when adding imidazole to series **1** and **2**.

Another possible explanation for the lowering of $V_{DB}V_{BA}$ could be different reduction and oxidation sites of AuP^+ and $AuP^\bullet$, respectively. As argued above, the initial reduction could be to a transient porphyrin ligand-located radical state, whereas the oxidation of the $AuP^\bullet$ radical might be from the reduced

(34) Paddon-Row, M. N. In *Electron Transfer in Chemistry*, 1st ed.; Balzani, V., Ed.; Wiley-VCH: Weinheim, 2001; Vol. 3, pp 201−215.
(35) It should be noted that imidazole will alter the driving force for both CR and CS as the oxidation potential and the E_{00} value for ZnP change, but that has been accounted for in the calculations of V_{DA}.
(36) Kasper, P.; Jensen, U. R. *ChemBioChem* **2003**, *4*, 413−424.
(37) Kadish, K. M.; Wenbo, E.; Ou, Z. P.; Shao, J. G.; Sintic, P. J.; Ohkubo, K.; Fukuzumi, S.; Crossley, M. J. *Chem. Commun.* **2002**, 356−357.

central metal ion.[37] Such a redistribution of charge would facilitate the CS step at the cost of slower rates for CR.

Considerations of the electron density distribution of the HOMO and LUMO of the electron donor as well as the distributional change of the electron density of the radical species are thus crucial when constructing model systems with the high CS/CR rate constant ratio which is needed to be able to achieve long-lived charge-separated states.

Acknowledgment. This work was supported by grants from the Swedish Research Council, the Knut and Alice Wallenberg Foundation, and the Hasselblad Foundation.

Supporting Information Available: The redox potentials of the studied molecules. This material is available free of charge via the Internet at http://pubs.acs.org.

JA066346C